Supporting Information for:

Electrical, Photoelectrochemical and Photoelectron Spectroscopic Investigation of the Interfacial Transport and Energetics of Amorphous TiO_2/Si Heterojunctions

Shu Hu[1,2†], Matthias H. Richter[1,2†], Michael F. Lichterman[1,2],

Joseph Beardslee[2,4], Thomas Mayer[5], Bruce S. Brunschwig[1] and Nathan S. Lewis*[,1,2,3]

[1]Division of Chemistry and Chemical Engineering, California Institute of Technology, Pasadena, CA 91125, USA.

[2]Joint Center for Artificial Photosynthesis, California Institute of Technology, Pasadena, CA 91125, USA.

[3]Kavli Nanoscience Institute, California Institute of Technology, Pasadena, CA 91125, USA.

[4]Lawrence Berkeley National Laboratory, Berkeley, CA 94720, USA.

[5]Darmstadt University of Technology, Materials Science Department, Petersenstrasse 32, 64287 Darmstadt, Germany.

*Corresponding author: nslewis@caltech.edu

† These authors contributed equally to this work.

Calculations of Band-Energy Diagrams

For intrinsic Si, the band gap (E_G = 1.12 eV), the electron affinity (χ = 4.07 eV), and the binding-energy difference between the VBM and the Si 2p CLBE (Si^0) of 98.74 eV, are well documented in the literature [1]. While a chemical shift of 3.8 eV for Si^{4+} of thermally grown SiO_2 is reported [2], the measured chemical shift of nominal Si^{4+} from the sub-oxides at Si/TiO_2 interfaces may vary from this value. Using the doping density obtained by 4-point probe resistivity measurements and the literature values above, the positions of the VBM, the conduction band minimum (CBM), the vacuum level (work function), and the Si 2p CLBE, relative to the Fermi level were calculated for bulk n-Si, n^+-Si, and p^+-Si according to Figure S3a, respectively. For clarity, literature and calculated values are marked with a single (*) and double asterisk (**), respectively in the band-energy diagrams (Figures 6, 7, and S6).and the following paragraphs. All other values were obtained directly from the XPS or UPS measurements, unless stated otherwise.

In the band-energy diagrams, the magnitude of the band bending (E_{BB}) in the Si space-charge region (SCR) at the respective interface is given by the difference of the calculated bulk position of the Si^0 2p CLBE (**) and the measured position of the Si^0 2p from XPS according to Figure S3b. The SiO_2 band line up of the RCA-2 treated Si surface (compare Figure S3c for x=1 and y=0), which was covered with a thin surface layer of native SiO_2, was calculated based on the position of the Si 2p core level for the surface oxide layer, i.e. the Si_{ox} photoemission line obtained by XPS, as well as using the measured VBM and work function (position of the secondary electron cutoff) of native SiO_2 obtained from UPS. For the thin Si_{ox} layers the values of the core level binding energy, the VBM and the work function that are determined by XPS

and UPS represent the averaged values over the thin oxide layer, i.e. are valid for core levels in the middle of the layer, as indicated in the graph.

Error of XPS Measurements

Two sources of error will be discussed: One is the error of the absolute peak position, which is included in the error bars in the two graphs Fig. 5 and S4 for the relative change of the absolute binding energy between the several samples; the other error is associated with determination of the relative peak shift of a single sample.

When taken from a sample, the error of the absolute peak position can be on the order of ±0.1 eV. On the other hand, the relative peak shift, e.g. the binding energy difference of metallic (Si^0) and oxidized Silicon (Si_{ox}) or the difference of the binding energy of bulk silicon and silicon at the surface in a sample can be determined with high precision. The latter is mainly determined by the uncertainty of peak fitting and data quality, e.g. the signal-to-noise ratio.

The error of absolute peak positions can be statistically reduced by multiple measurements of samples prepared in the same manner, as was performed in this study (> 10 times). The error of the relative peaks shifts, i.e. the quality of peak fitting, can be reduced statistically in the same manner by improving the signal-to-noise ratio of the measurement.

For example, the value of 0.06 eV (which is the band bending in n^+-Si in Fig. S6) is calculated based on a relative peak shift of two peaks, the bulk binding energy value of Si and its value at the surface. Here the Si^0 2p peak can be fitted with two components (bulk and surface) and the relative difference in binding energy is 0.06 eV which has a much lower error than values obtained from absolute peak positions of different samples.

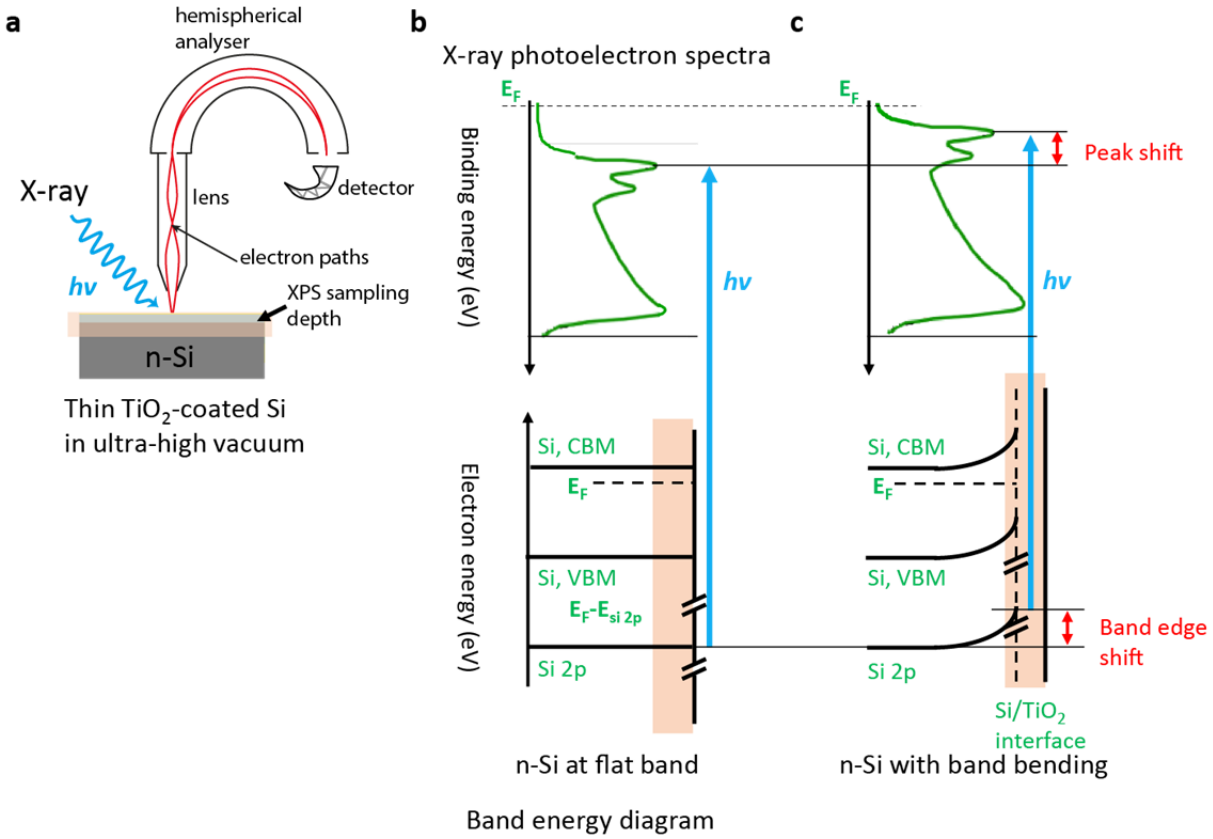

Figure S1: Correlation between the band-energy diagram and X-ray photoelectron spectra (XPS) for n-Si. (a) The XPS sampling depth is indicated in surface region of a thin TiO_2-coated Si sample. Correspondingly, the band-edge shift (labeled in red) for n-Si from flat-band conditions (b) to depletion conditions (c) causes a shift (labeled in red) in the peak for the core-level binding energy (CLBE) corresponding to Si 2p photoemissions ($E_{Si\ 2p}$). In (b) and (c), CBM and VBM indicate the positions of the Si conduction-band minima and valence-band maxima, respectively, and E_F indicates the Fermi level for the Si.

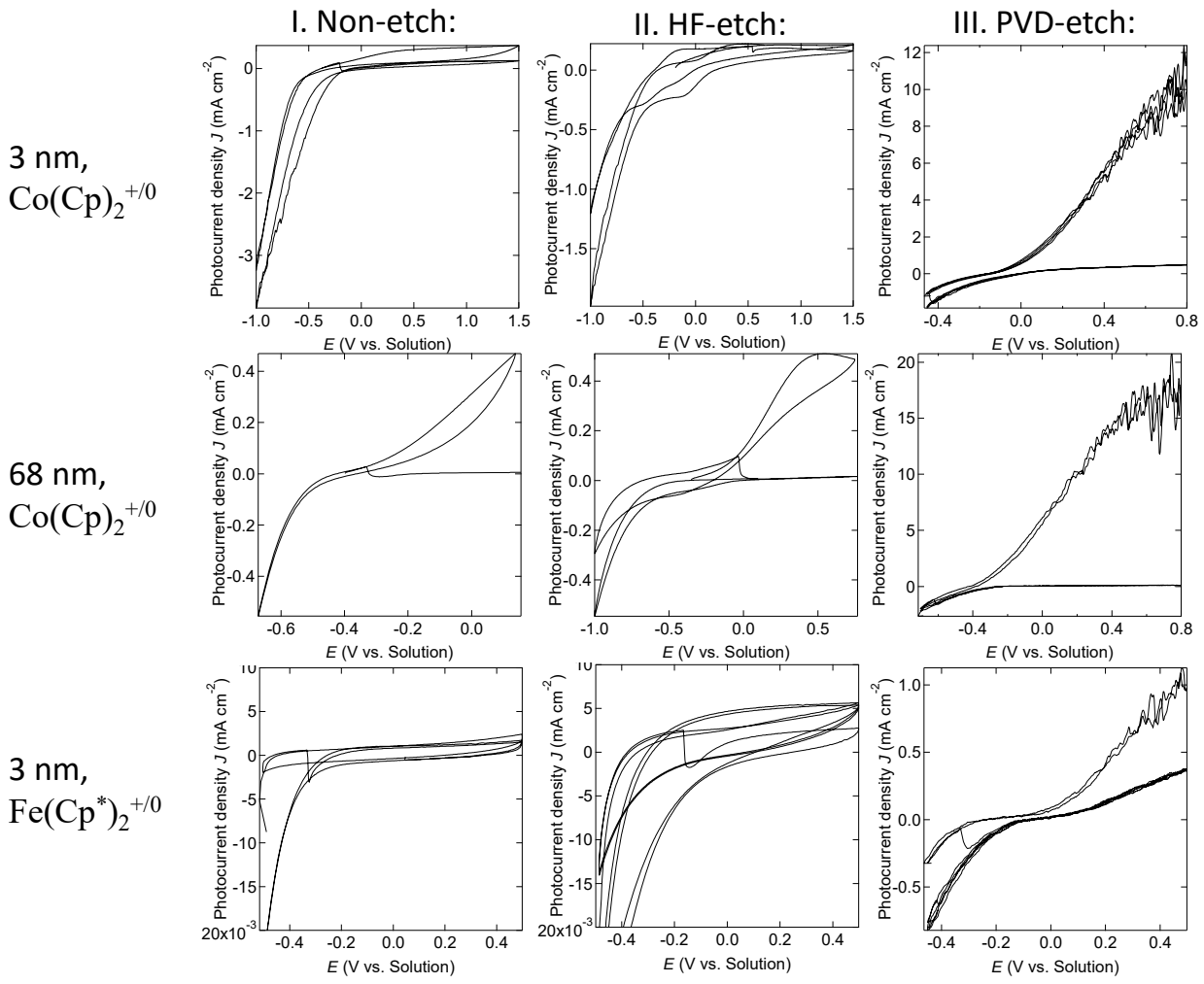

Figure S2: Two consecutive photoelectrochemical current density versus potential (*J*-*E*) scans for n-Si/TiO_2 photoelectrodes in contact with non-aqueous electrolytes containing $Fe(Cp^*)_2^{+/0}$ or $Co(Cp)_2^{+/0}$ redox couples under illumination and in dark, respectively. Non-etch refers to as-grown TiO_2; HF-etch refers to TiO_2 surfaces treated with hydrofluoric acid etching; PVD-etch refers to metallized TiO_2 surfaces treated by Ar plasma etching which facilitates charge transfer. As-grown TiO_2 surfaces, as well as HF-etched and RIE-etched surfaces, did not facilitate charge transfer to liquid electrolytes at positive potentials, whereas metallized TiO_2 surfaces readily passed anodic current.

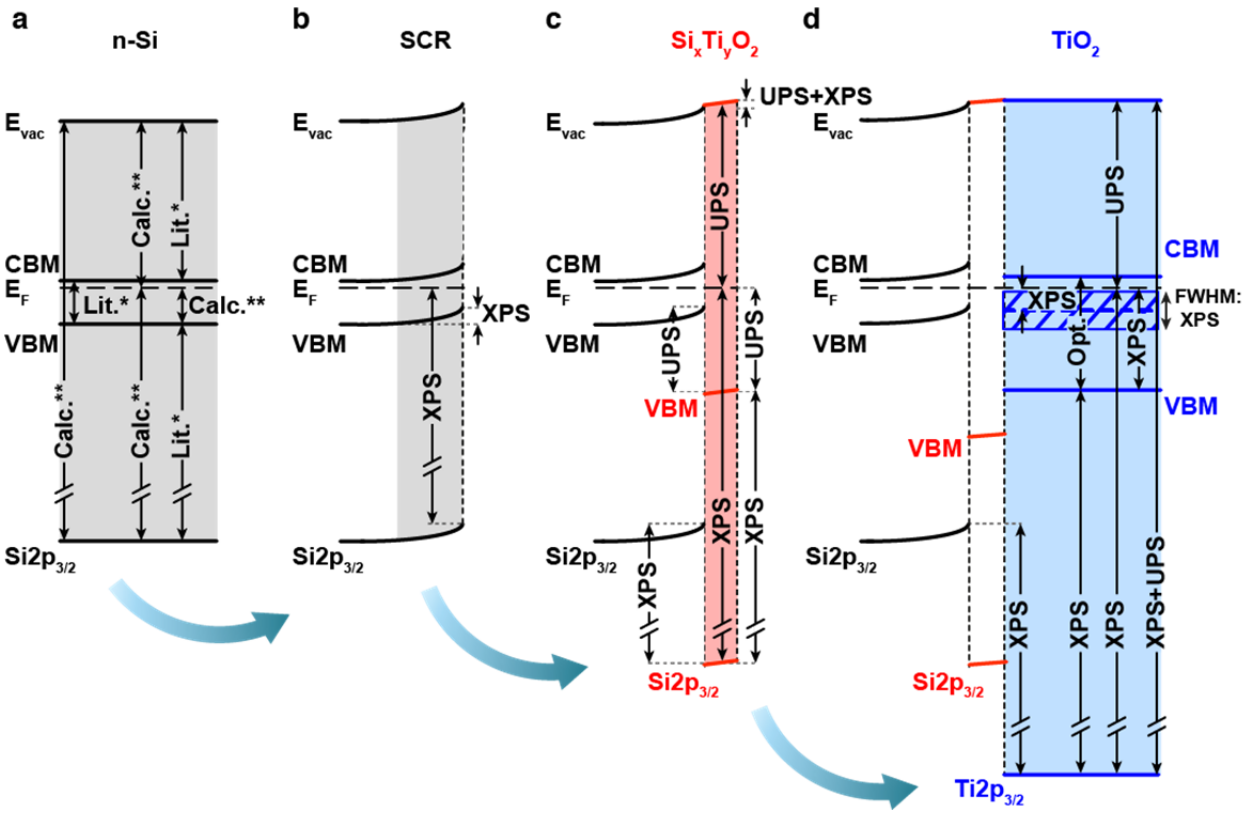

Figure S3: Development of energy-band relationships from UPS and XPS measurements. Literature values, marked with a single asterisk (*), are the intrinsic electron affinity, band gap and the difference in energy between the observed binding energy of the top of the valence band (VBM) and the core-level binding energy (CLBE) of Si. Calculated values, marked with a double asterisk (**), were derived from the doping density, which was obtained from 4-point probe resistivity measurements. All other values, if not stated otherwise, were obtained from XPS and UPS measurements. The development of an interfacial band diagram is illustrated progressively: (a) the energy-band relations for bulk silicon; (b) adds the band bending in the space-charge (SCR) region of Si; (c) adds the $Si_xTi_yO_2$ interfacial layer (for SiO_2, x=1, y=0); and finally, (d) adds the TiO_2 overlayer. The optical (Opt.) band gap of TiO_2 was measured separately (from Fig. S14 in Hu et al.[3]).

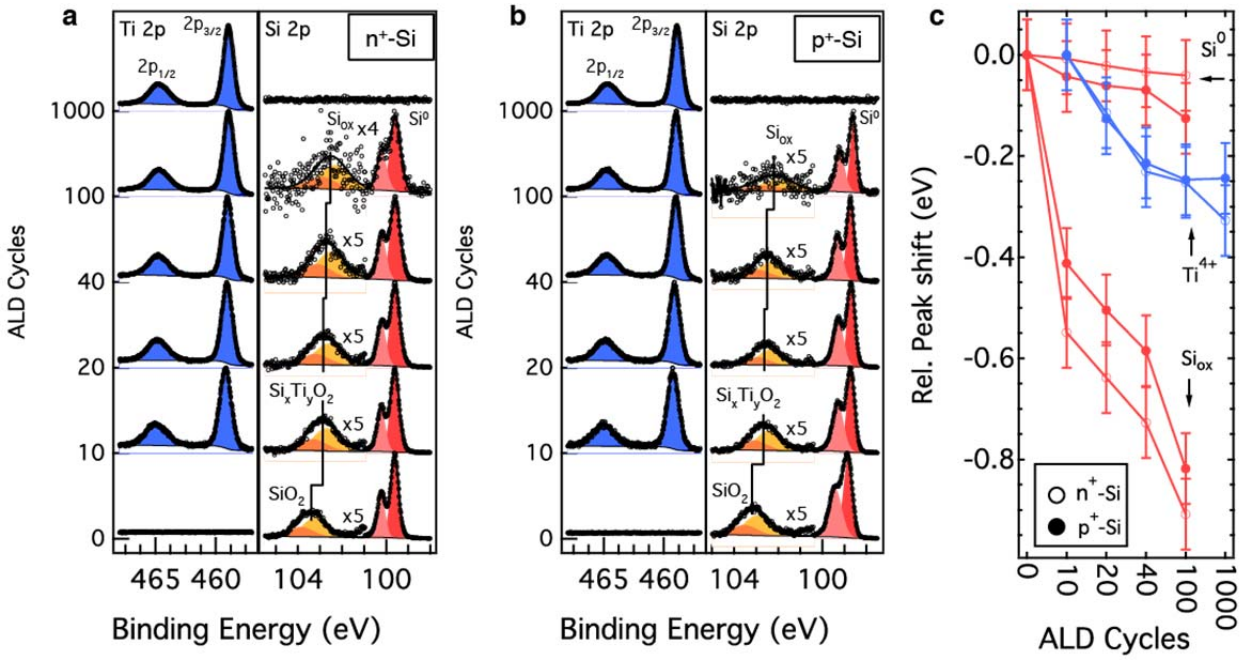

Figure S4: Raw data and fitted peaks for (a) the Ti 2p core-level XPS spectra and the Si 2p core-level spectra of ALD TiO_2 grown on n^+-Si and (b) the Ti 2p core-level XPS spectra and the Si 2p core-level spectra of ALD TiO_2 grown on p^+-Si. The Si_{OX} component was magnified by the given number. The fitted peaks for the Ti 2p levels of TiO_2, the Si 2p levels of Si and the oxides of Si are shown. (c) Relative energy position of the Si oxide peak shift Si_{ox}, Ti 2p peak Ti^{4+} and Si^0 peak shift with a change of chemical shift for Si_{ox} from 3.8 eV* for SiO_2 to 3.09 eV±0.1 eV from 0 to 10 ALD cycles for n^+-Si (open circles) and p^+-Si (solid circles).

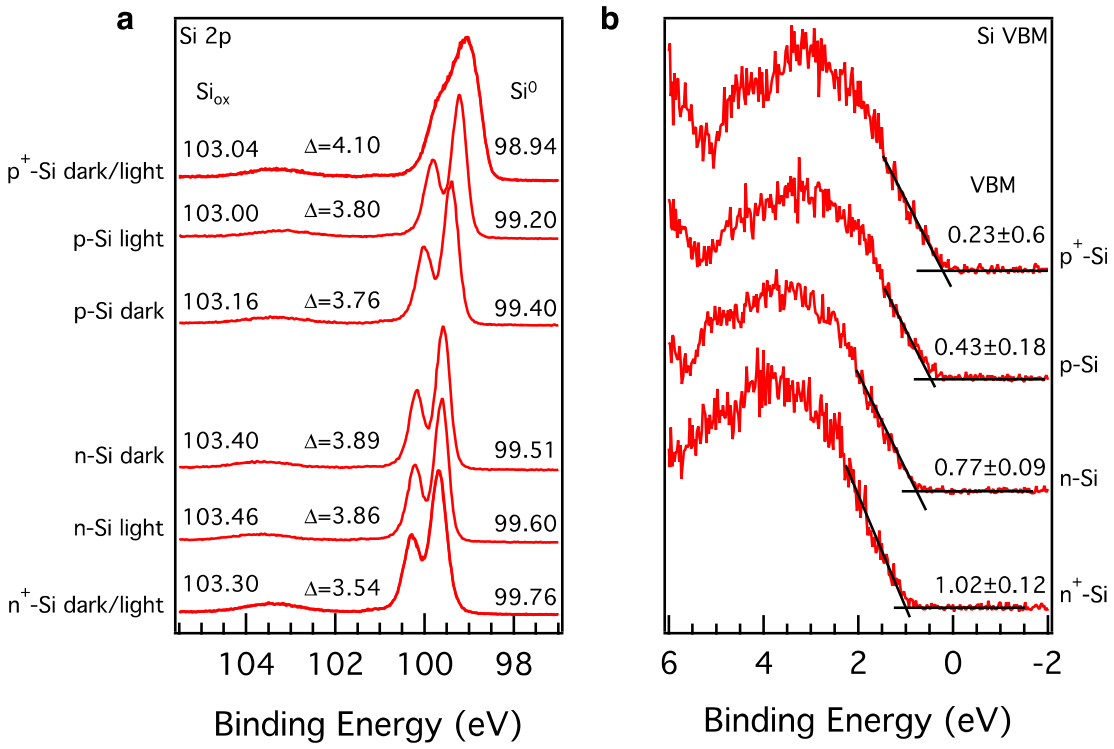

Figure S5: XPS characterization of RCA-2 treated n^+-Si and p^+-Si surfaces prior to ALD. Si 2p core-level spectra (a) for p^+-, p-, n-, and n^+-Si are shown in the dark (15 W X-ray power) and light (150 W X-ray power) with core-level emission positions for Si^0 and Si_{ox}. The delta value gives the difference between Si^0 and Si_{ox}. XPS valence-band spectra (b) for p^+-, p-, n-, and n^+-Si are shown with indicated valence-band maximum for Si.

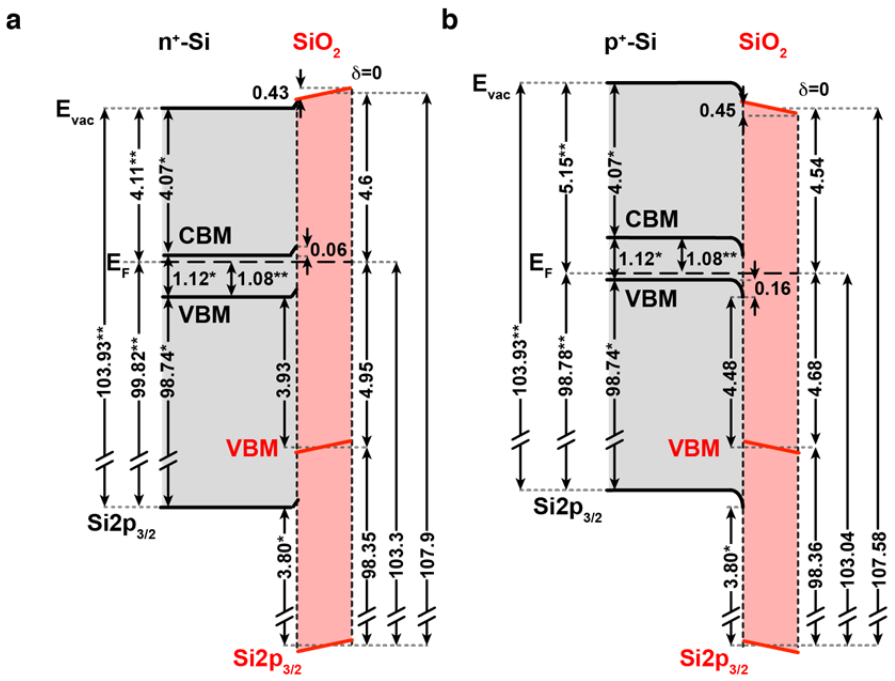

Figure S6: Band energy diagrams of n^+-Si and p^+-Si surfaces after RCA-2 treatments prior to ALD. The literature [1] and calculated values are marked with a single, *, and double asterisk, **, respectively (see text). Values below E_F are taken from XPS measurements and the work function is obtained by UPS. All numeric values are in eV.

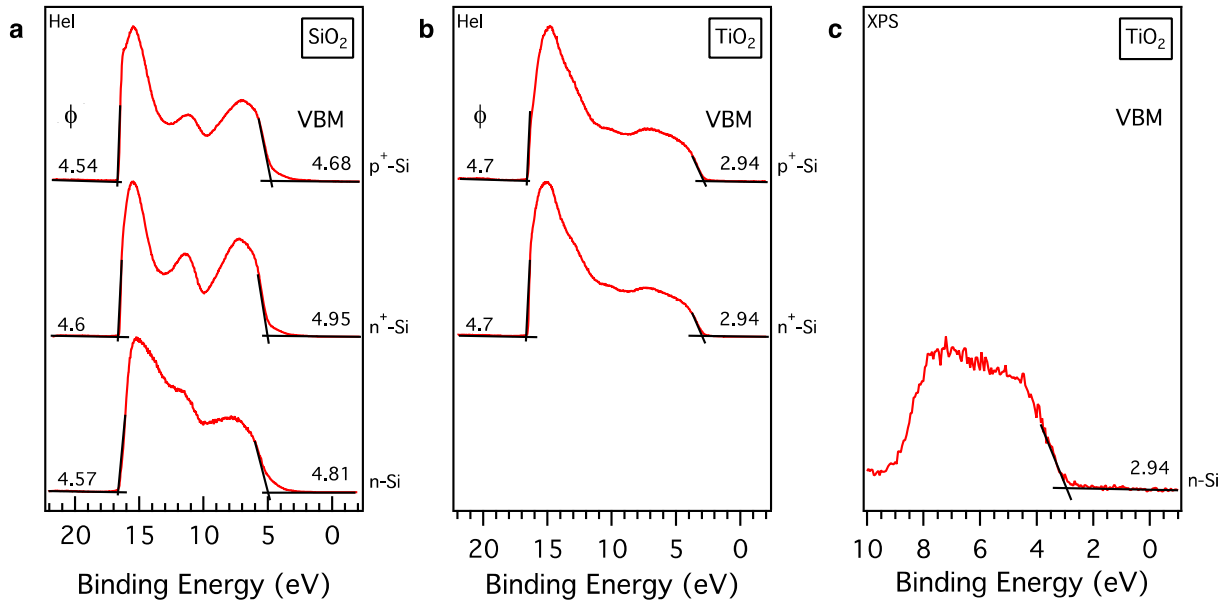

Figure S7: (a) UPS spectra of n-Si, n^+-Si, and p^+-Si with native oxide formed after RCA-2 treatment. (b) UPS spectra of n^+-Si and p^+-Si after 100 ALD cycles of TiO_2 (c). XPS VBM spectra of n-Si after 150 cycles ALD of TiO_2. The work function is given by the photon energy minus the binding energy of the secondary electron cutoff: $\phi = 21.21\ \text{eV} - E_B$ for (a) and (b). The VBM is directly given when plotted against the binding energy (c).

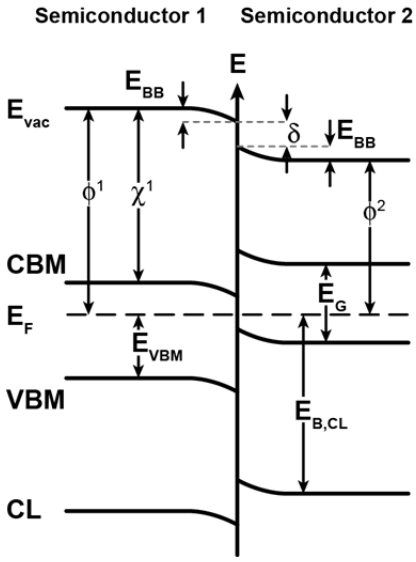

Figure S8: Diagram showing the specific energies: the material work function ϕ^1 and ϕ^2, the electron affinity χ, the core level binding energy $E_{B,CL}$, the magnitude of the band bending E_{BB}, and the interface dipole δ.

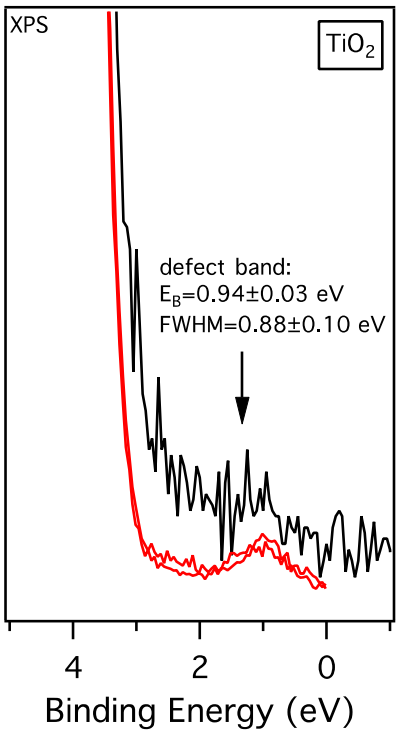

Figure S9: XPS valence band spectra of as-grown ALD TiO_2 reproduced from Lichterman *et al.*[4] (red) overlaid with data from the same sample in Figure S7b (black). The position and FWHM of the defect band were obtained from its fitting, i.e. a binding energy of 0.94 ± 0.03 eV and a FWHM of 0.88 ± 0.10 eV.

References:

(1) Gleason-Rohrer, D. C.; Brunschwig, B. S.; Lewis, N. S. Measurement of the Band Bending and Surface Dipole at Chemically Functionalized Si(111)/Vacuum Interfaces. *J. Phys. Chem. C* **2013**, *117*, 18031–18042.

(2) Kobayashi, H.; Kubota, T.; Kawa, H.; Nakato, Y.; Nishiyama, M. Oxide Thickness Dependence of Energy Shifts in the Si 2p Levels for the SiO_2/Si Structure, and Its Elimination by a Palladium Overlayer. *Appl. Phys. Lett.* **1998**, *73*, 933.

(3) Hu, S.; Shaner, M. R.; Beardslee, J. A.; Lichterman, M.; Brunschwig, B. S.; Lewis, N. S. Amorphous TiO_2 Coatings Stabilize Si, GaAs, and GaP Photoanodes for Efficient Water Oxidation. *Science* **2014**, *344*, 1005–1009.

(4) Lichterman, M. F.; Hu, S.; Richter, M. H.; Crumlin, E. J.; Axnanda, S.; Favaro, M.; Drisdell, W.; Hussain, Z.; Mayer, T.; Brunschwig, B. S.; et al. Direct Observation of the Energetics at a Semiconductor/liquid Junction by Operando X-Ray Photoelectron Spectroscopy. *Energy Environ. Sci.* **2015**, *8*, 2409–2416.